Bussetta *et al. Adv. Model. and Simul. in Eng. Sci.(2015)2:27*
DOI 10.1186/s40323-015-0048-2

Advanced Modeling and Simulation in Engineering Sciences
a SpringerOpen Journal

RESEARCH ARTICLE Open Access

3D numerical models using a fluid or a solid formulation of FSW processes with a non-cylindrical pin

Philippe Bussetta[1], Narges Dialami[2], Michele Chiumenti[2], Carlos Agelet de Saracibar[2], Miguel Cervera[2], Romain Boman[1] and Jean-Philippe Ponthot[1*]

*Correspondence: jp.ponthot@ulg.ac.be
[1]Department of Aerospace and Mechanical Engineering, Non Linear Computational Mechanics, University of Liège, Quartier Polytech 1, Allée de la Découverte 13a, 4000 Liège, Belgium
Full list of author information is available at the end of the article

Abstract

Friction stir welding process is a relatively recent welding process (patented in 1991). FSW is a solid-state joining process during which materials to be joined are not melted. During the FSW process, the behaviour of the material is at the interface between solid mechanics and fluid mechanics. In this paper, a 3D numerical model of the FSW process with a non-cylindrical tool based on a solid formulation is compared to another one based on a fluid formulation. Both models use advanced numerical techniques such as the Arbitrary Lagrangian Eulerian formulation, remeshing or the Orthogonal Sub-Grid Scale method. It is shown that these two formulations essentially deliver the same results.

Keywords: Friction stir welding (FSW), Finite element method, Remeshing, Arbitrary Lagrangian Eulerian (ALE) formalism

Background

Friction stir welding (FSW) is a relatively recent welding process, which was developed at the Welding Institute (UK) and patented in 1991 [1]. FSW is a solid-state joining process. It means that during welding the materials to be joined are not melted. The joining is constituted by mechanical intermixing of the two materials. A rotating non-consumable tool is inserted between the two work-pieces and displaced along the welding direction (see Fig. 1). The tool is composed of two parts: a pin and a shoulder. The pin is introduced into the welded joint to mix deeply the two materials together. The aim of the shoulder is to contain the material around the pin. The part of the welding joint where the velocity of the tool and the advancing velocity add up is named the advancing side. The other part, where the two velocities are in opposite directions, is called the retreating side. The friction between the rotating tool and the work-pieces as well as the plastic deformation in the neighbourhood of the tool increase the temperature in the welded zone and thus soften the materials. But, during the process, the temperature is always smaller than the melting temperature of the materials. So, the heat-affected zone is smaller and the quality of the welding is higher than in more classical welding processes. In spite of the important number of applications of FSW, the phenomena happening during welding are still not very well understood. Therefore, the investigations on this process and especially

© 2015 Bussetta et al. This article is distributed under the terms of the Creative Commons Attribution 4.0 International License (http://creativecommons.org/licenses/by/4.0/), which permits unrestricted use, distribution, and reproduction in any medium, provided you give appropriate credit to the original author(s) and the source, provide a link to the Creative Commons license, and indicate if changes were made.

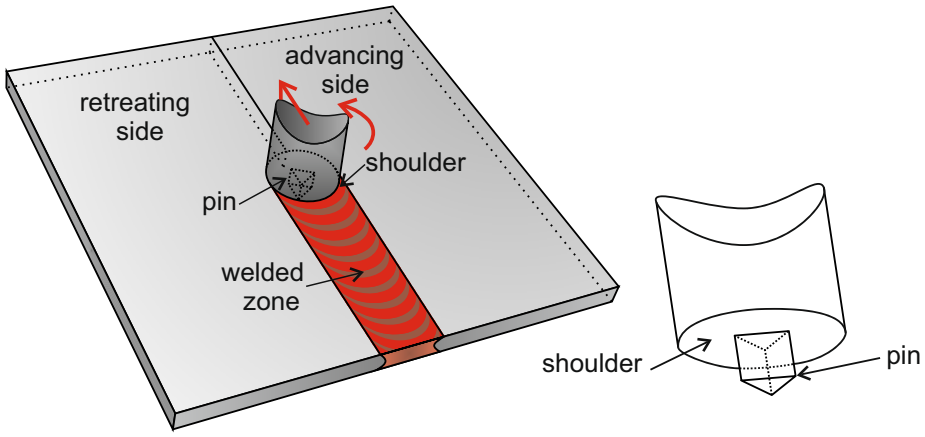

Fig. 1 Scheme of the FSW process

regarding numerical simulations are still very active [2–8]. From the numerical modelling point of view, a bibliography review is presented by He et al. [9], by Dialami et al. [10] and by Bussetta et al. [11]. Recently, the FSW process has been used to weld different material types, such as steel in Toumpis et al. [12], magnesium in He et al. [13] even polymers in Simões and Rodrigues [14]. The mechanical intermixing induces very high strains in the material in the neighbourhood of the tool. Using a classical Lagrangian formulation as it is generally the case in solid mechanics would thus inevitably lead to mesh distortion. Consequently, classical numerical simulation techniques have to be extended in order to track the correct material deformations. One of the possibilities is to use the Arbitrary Lagrangian Eulerian (ALE) formulation [15–18]. This formulation is used to keep the mesh motion under control regardless of the real material displacements. The ALE formulation is also used to maintain a good mesh quality during the computation.

This paper deals with the extension to 3D of the works exposed in [11]. This article presents and compares two different 3D numerical approaches of the FSW process. The first model is based on a solid approach written in terms of nodal positions and nodal temperatures. The second model is based on a fluid approach written in terms of the velocity, the pressure and the temperature fields. Both models use advanced numerical techniques such as remeshing and the ALE formulation. 2D models are useful to test and easily compare both numerical formulations. Nevertheless, the FSW process is a fully 3D thermomechanical process. The effect of the shoulder and the thermal boundary conditions have a great influence on the FSW process, but they cannot be considered in the 2D models.

This article is split into three parts. First, both 3D numerical approaches are presented. Secondly, the 3D models are compared and the differences with the 2D models are exposed. Finally, some conclusions and explanations about the differences between the results of both models are made.

3D numerical modelling of FSW process

To model this welding process, the displacement of the tool is split into an advancing movement (actually assigned to the work-pieces but, in the opposite direction) and a rotation (imposed to the tool). In other words, the centre of the pin is fixed and a constant velocity is imposed to the plates (see Fig. 2).

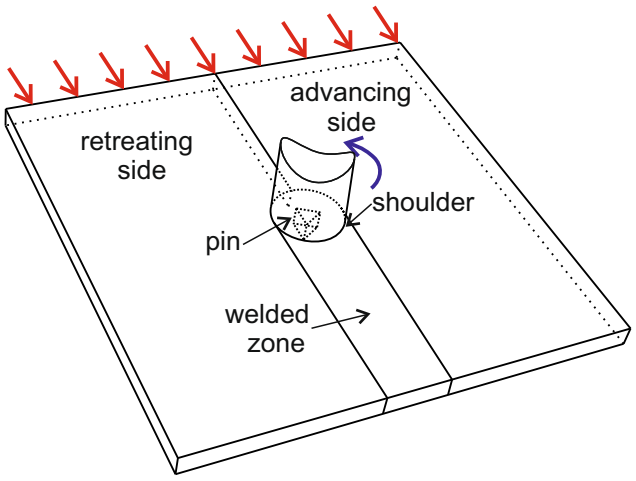

Fig. 2 Scheme of the FSW model. A rotation is imposed to the pin (*blue arrow*) while the advancing velocity of the pin is replaced by a velocity imposed to the plates in the opposite direction (*red arrows*)

The tool is described by a classical Lagrangian mesh. Due to high deformations in the neighbourhood of the tool, the use of a Lagrangian formalism would lead very quickly to mesh entanglement. Then, the plates are modelled using the ALE formulation. On top of this, the ALE formulation allows the model to take into account tools with no rotational symmetry. In relation with the distance from the rotation axis of the tool, the plates are split in three zones. In the closest zone around the tool (red region in Fig. 3), the mesh has the same rotational speed as the tool. In the model, this region is limited by the value of the distance from the rotation axis of the tool equal to the value of the radius of the shoulder. In the furthest zone from the tool, the grey zone in Fig. 3, the mesh is fixed and the material is flowing through the mesh. The last zone is a transition zone, white region numbered 2 in Fig. 3. This zone connects the meshes of both other zones. Therefore, the quality of the

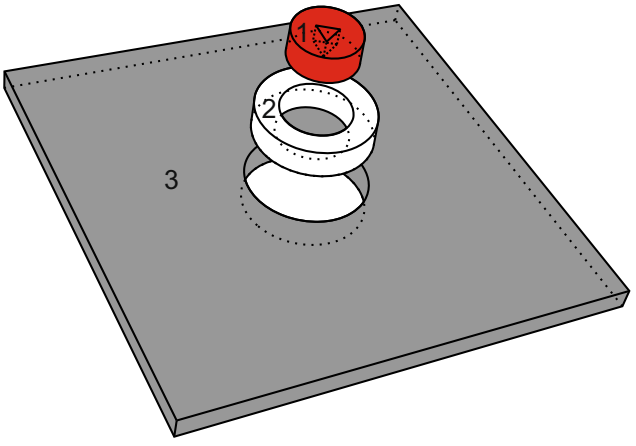

Fig. 3 Scheme of the different zones of the numerical model. The different zones of the model: ALE formulation is used on the red region (*1*), the transition zone corresponds to the white region (*2*), and the Eulerian formulation is applied on the grey region (*3*)

mesh in this zone decreases with the simulation time. The numerical techniques used to overcome this problem are explained in the section named "The transition zone".

Thermomechanical formulation

The numerical models presented here are based on the finite element method. In this paper, two numerical formulations are compared (for more information about these formulations see [11]). The first one is based on a solid mechanics approach. It is written in terms of nodal positions and temperatures. The second one is based on a fluid mechanics approach. The equilibrium is written as a function of nodal velocities, pressures and temperatures.

Solid approach

The position and temperature fields are computed at each node of the elements. The mesh is composed of 21,980 linear hexahedral elements. The stresses and the internal variables are computed at each quadrature point of the element (8 Gauss points). To overcome the locking phenomenon, the pressure is considered constant over the element and computed only at a central quadrature point. The thermomechanical equations are split into a mechanical part and a thermal part. At each time step, the mechanical equations are first solved using a constant temperature field. This temperature field is the one obtained at the previous increment. Then, the thermal equations are solved on the frozen resulting geometrical configuration that has just been obtained.

Fluid approach

The fluid approach is based on a stabilized mixed linear temperature-velocity-pressure finite element formulation. This formulation is stabilized adopting the Orthogonal Sub-Grid Scale method (OSS) [19–21] to solve both the pressure instability induced by the incompressibility constraint and the instabilities coming from the convective term. A mesh of 74,127 linear tetrahedral elements is used for the domain discretisation. The velocity, the pressure and the temperature fields are computed at each node of the elements. The deviatoric stresses and the other internal variables are computed at each quadrature point of the element. Finally, the coupled thermomechanical problem is solved by means of a staggered time-marching scheme where the thermal and mechanical sub-problems are solved sequentially, within the framework of the classical fractional step methods [22,23].

The transition zone

Solid approach

In the solid approach, the transition zone is a ring with a finite thickness (region 2 in Fig. 3). In this region, the evolution of the rotational speed of the mesh, which differs from the material velocity, is linearly interpolated between the ALE region and the Eulerian zone. As the mesh distortion grows with time, a remeshing operation is periodically required. The remeshing operation can be divided into two steps. First, a better-suited mesh, called the new mesh, is created. In this case, the simple geometry of this region allows an easy generation of the new hexahedral mesh. Then, to carry on the computation over this new mesh, the data are transferred from the old mesh to the new one (for more informations about the data transfer see [24]).

Fluid approach

In the fluid model the transition zone (region 2 in Fig. 3) is limited to a tube of zero wall thickness. Each node of this zone is duplicated. One node is linked to the ALE region (numbered 1) and the other one to the Eulerian region (numbered 3). The coupling between both regions is performed using a specific node-to-node link approach. In this case the ALE mesh would slide precisely from one Eulerian interface node to the next one at each time step.

Thermomechanical constitutive model

In both models, the constitutive model of the tool is thermo-rigid. So, no mechanical fields are computed over this material. However, from the point of view of the thermal equations, the tool has a classical thermal behaviour as far as heat conduction is concerned. In addition, the material behaviour of the plates is modelled as thermo-visco-plastic using a Norton-Hoff constitutive model:

$$\boldsymbol{S} = 2\mu(T)\widehat{\boldsymbol{D}}\left(\sqrt{3}\sqrt{\frac{2}{3}\widehat{\boldsymbol{D}}:\widehat{\boldsymbol{D}}}\right)^{m(T)-1} \tag{1}$$

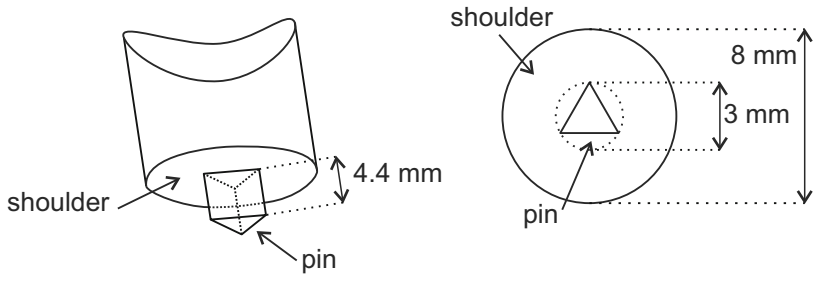

Fig. 4 Scheme of the tool

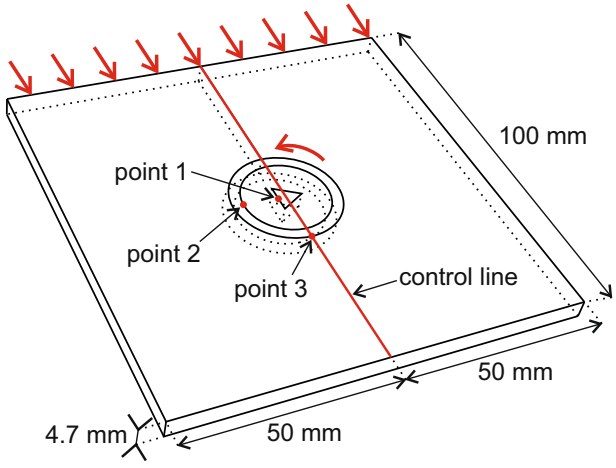

Fig. 5 Scheme of the model with the initial position of the control point and the control line

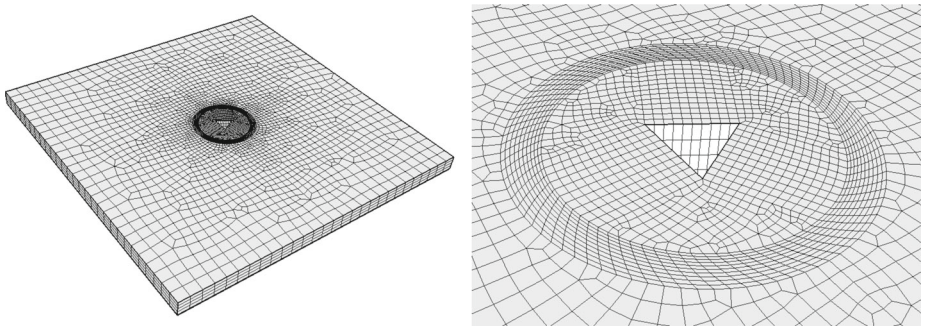

Fig. 6 Initial quadrangular mesh (21,980 elements) used in the solid model. Global view and zoom around the tool position

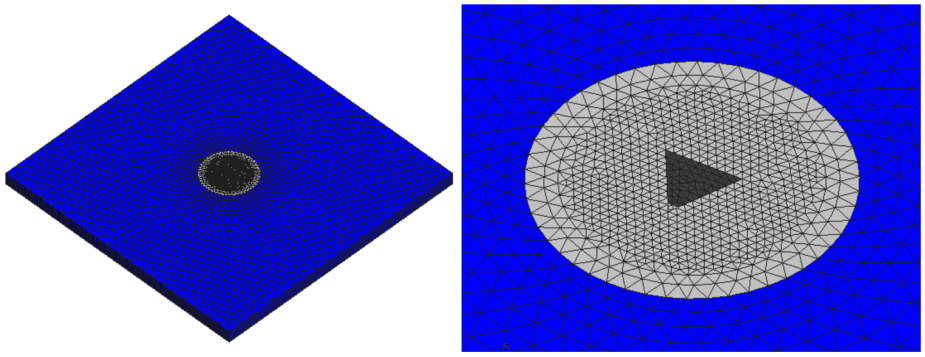

Fig. 7 Initial tetrahedral mesh (74,127 elements) used in the fluid model. Global view and zoom around the tool position

where m and μ are the strain rate sensitivity and viscosity parameters respectively. Both are temperature dependent. $\boldsymbol{S}$ is the Cauchy stress deviator tensor and $\widehat{\boldsymbol{D}}$ is the deviatoric part of the strain-rate tensor.

In the FSW process, the heat is mostly generated by the mechanical dissipation, which is computed as a function of the plastic strain rate and the deviatoric stresses as:

$$D_{mech} = \gamma \boldsymbol{S} : \widehat{\boldsymbol{D}} \tag{2}$$

where $\gamma \approx 0.9$ is the fraction of the total plastic energy converted into heat.

Solid approach

In the solid model, the value of the variation of the pressure (dp) is computed thanks to the variation of the volume (dV) and the bulk modulus (K): $dp = KdV$. In addition, with the solid approach, it is possible to replace the Norton-Hoff constitutive model with a thermo-elasto-visco-plastic one, see e.g. [25]. With this kind of constitutive model, it is possible to compute the residual stresses.

Fluid approach

In the fluid model, the material is assumed to be incompressible and this constraint is incorporated into the equations to be solved.

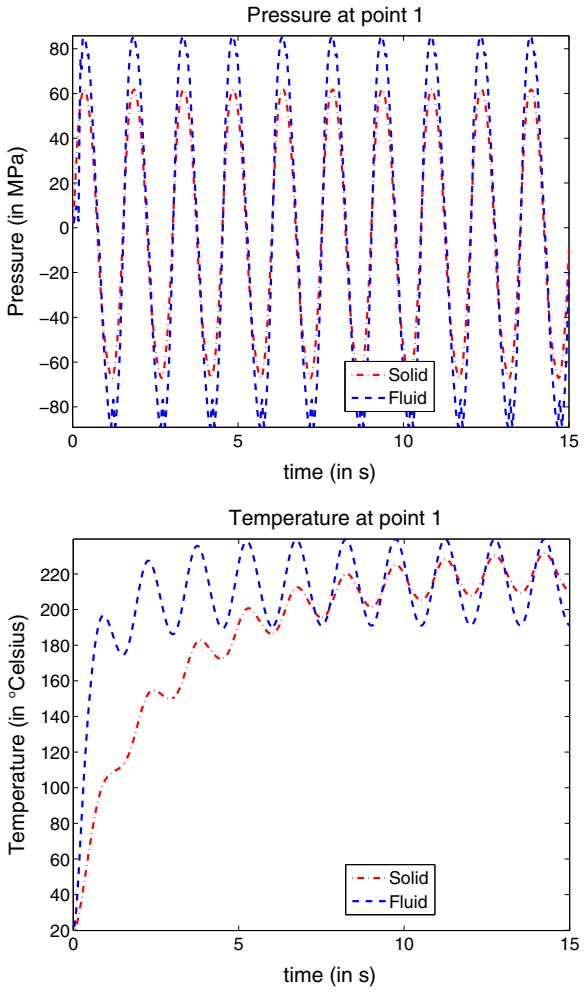

Fig. 8 Evolution of the pressure and the temperature computed by the two models at the control point 1 (rotating with the tool). The rotation speed of the tool is 40 RPM and the initial position of this point is defined in Fig. 5

Thermomechanical contact

A perfect sticking thermomechanical contact is considered between the tool and the work-piece. It means that the temperature field and the displacement field are continuous through the interface between the tool and the work-piece. Like some authors [26–28], we assume that the heat produced by the friction between the tool and the work-piece is negligible versus the heat generated by plastic deformations.

Comparison of numerical results

In this paper, the numerical results of the solid approach are compared with the already validated model based on the fluid approach (see [2,6,10,15]). In this example, the section of the pin is an equilateral triangle (Figs. 4, 5). The dimensions of the tool are presented in Fig. 4. The width of the two plates is 50 mm, the thickness is 4.7 mm and the simulated length is 100 mm. The rotation axis of the tool is located at the centre of the simulated region (see Fig. 5).

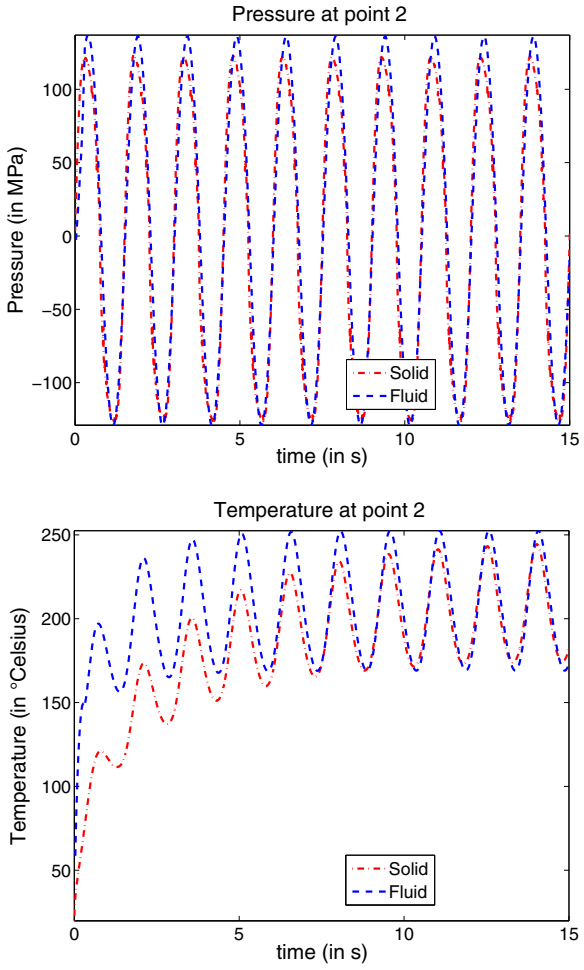

Fig. 9 Evolution of the pressure and the temperature computed by the two models at the control point 2 (rotating with the tool). The rotation speed of the tool is 40 RPM and the initial position of this point is defined in Fig. 5

The most important parameters of the considered FSW process are the rotation speed (40 RPM or 100 RPM) and the welding speed (400 mm min^{-1}). The thermomechanical properties of the plates are the following:

- density: 2700 kg m^{-3}
- bulk modulus: 69 GPa (used only with the solid approach)
- thermomechanical Norton-Hoff law (presented in the page 4) with $\mu = 100$ MPa, $m = 0.12$,
- heat conductivity: 120 W m^{-1} K^{-1}
- thermal expansion coefficient: 1×10^{-6} K^{-1}
- heat capacity: 875 J kg^{-1} K^{-1}

The thermomechanical properties of the tool are the following:

- density: 7800 kg m^{-3};
- heat conductivity: 43 W m^{-1} K^{-1};

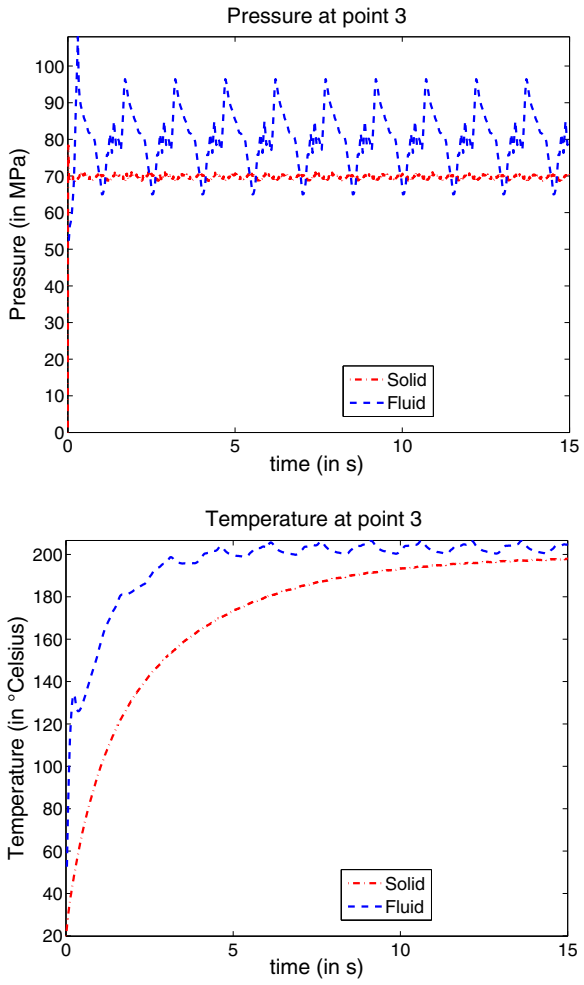

Fig. 10 Evolution of the pressure and the temperature computed by the two models at the control point 3 (fixed in space). The rotation speed of the tool is 40 RPM and the initial position of this point is defined in Fig. 5

- heat capacity: 460 J kg^{-1} K^{-1}.

During all the computation, the room temperature is considered constant at 20 °C. The thermal boundary conditions of this problem are the following (heat transfer is neglected along the external perimeter of the two plates):

- Conduction on the lower side of both plates (approximation of the thermal behaviour of the backing plate), exchange coefficient: 4500 W m^{-2} K^{-1};
- Convection and radiation on the free upper side of both plates (except the part in contact with the tool), convection coefficient: 10 W m^{-2} K^{-1}, emissivity coefficient: 0.2.

With the rotation speed of 40 RPM, the total time of the simulation is 15 s which corresponds to 10 revolutions for the tool. With the rotation speed of 100 RPM, the solution is computed for 20 revolutions for the tool (i.e. the total time of the simulation is 12 s).

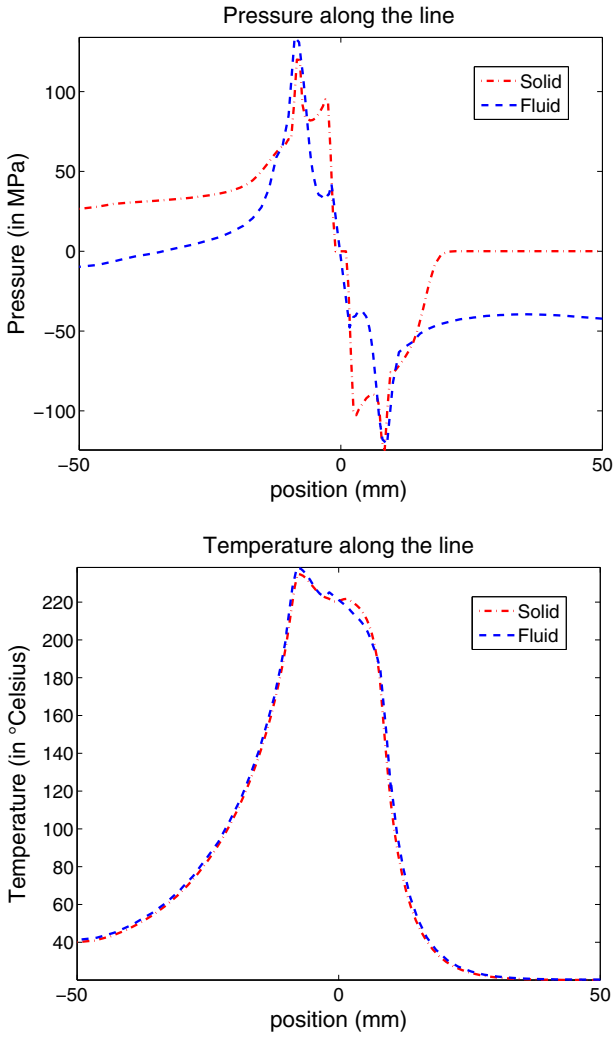

Fig. 11 Final values of the pressure and the temperature computed by the two models along the control line (i.e. after 15 s). The rotation speed of the tool is 40 RPM and the considered line is defined in Fig. 5

Figures 6 and 7 expose respectively the mesh of the solid model and the one of the fluid model. Figures 8, 9, 10 and 11 show the evolution of the pressure and the evolution of the temperature computed by the two models with the rotation speed of 40 RPM at the control points and along the control line defined in Fig. 5. Figures 12, 13, 14 and 15 present the same comparison with the rotation speed of 100 RPM. Points 1 and 2 have the same rotational speed as the tool (these points move according to the mesh). Point 3 is fixed in space.

After a transient phase which depends on the numerical strategy adopted for each approach the results of both models are very similar for the two values of the rotation speed of the tool (see Figs. 8, 9, 10, 12, 13, 14). The difference of frequency between the pressure at point 3 and the pressure and the temperature at points 1 and 2 is explained by the fact that point 3 is fixed in space while points 1 and 2 have the same rotational velocity as the tool. On the one hand, the pressure at point 3 is affected by the three corners of the pin. On the other hand, the frequency of the pressure and the temperature at points 1 and

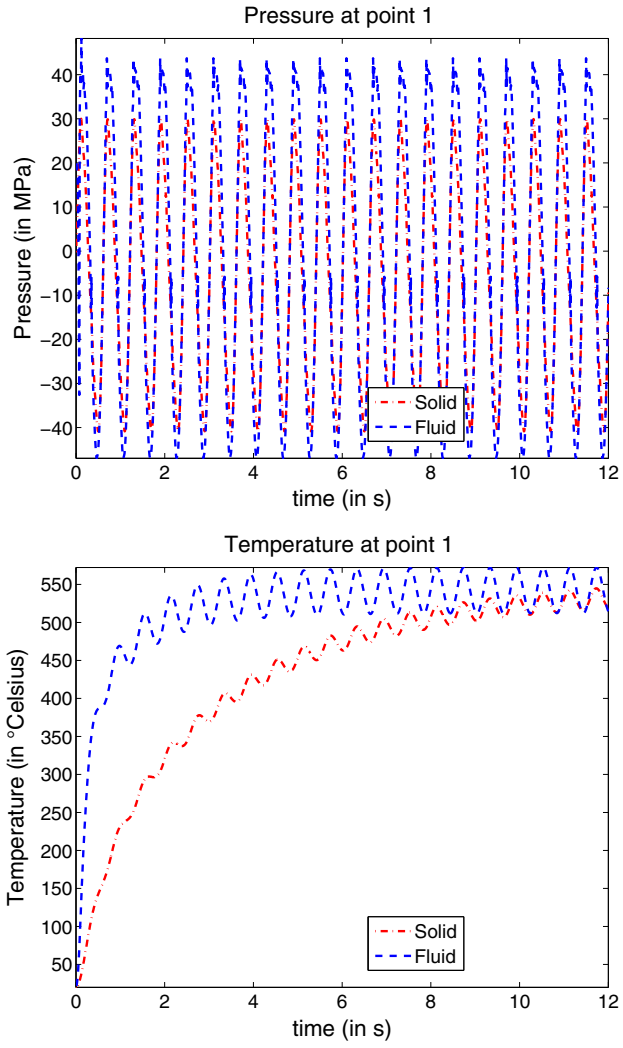

Fig. 12 Evolution of the pressure and the temperature computed by the two models at the control point 1 (rotating with the tool). The rotation speed of the tool is 100 RPM and the initial position of this point is defined in Fig. 5

2 are controlled by the rotation speed of the tool. Consequently, the pressure frequency at point 3 is three times higher than the frequency of the pressure or the temperature at points 1 or 2.

In addition, the temperature field is a good indicator of the mechanical intermixing of the material. The small differences between the values of the temperature fields along the control line (Figs. 11, 15) show that the two models essentially deliver the same results. The good agreement between the temperature field is confirmed thanks to the value of the temperature field on the top of the plates (see Figs. 16, 17 for a rotation speed of 40 RPM and Figs. 18, 19 for a rotation speed of 100). The small gap between the temperature fields can be explained by the differences between the element types used by both models. Moreover, the value of the pressure field is similar around the tool (see Figs. 11, 15). The difference between both formulations can explain an important part of the gap between the pressure field of both models. Indeed, the pressure is computed directly at the nodes

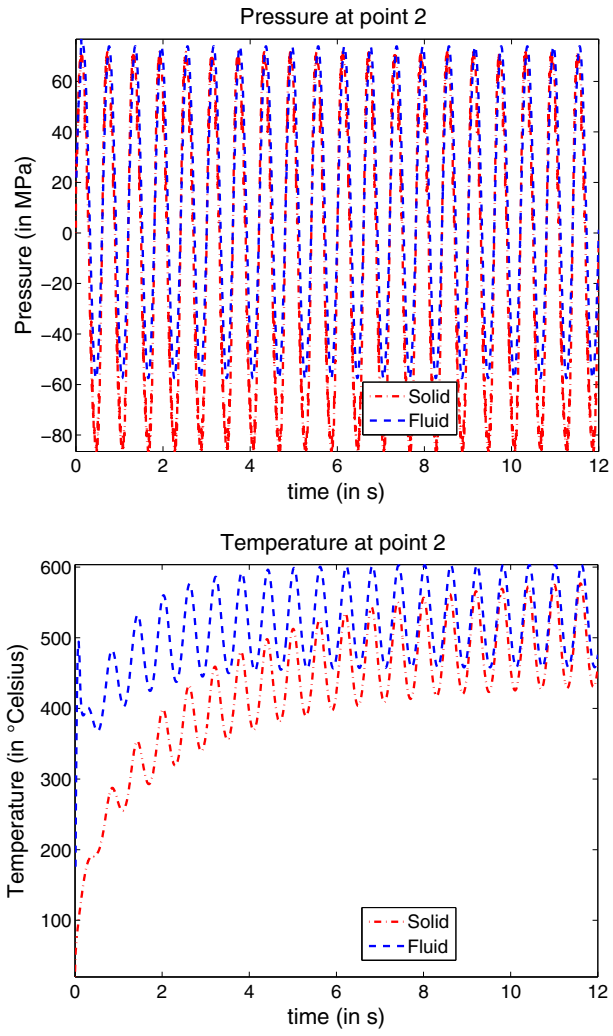

Fig. 13 Evolution of the pressure and the temperature computed by the two models at the control point 2 (rotating with the tool). The rotation speed of the tool is 100 RPM and the initial position of this point is defined in Fig. 5

with the fluid model and is evaluated at the location of the quadrature points with the solid model. Those values are then extrapolated to the nodes. These comparisons with two values of the rotation speed of the tool prove that the solid and the fluid models essentially deliver the same results as far as the temperature field and the pressure field prediction during welding are concerned. Nevertheless, from the point of view of CPU time, the fluid model is faster than the solid one (see Table 1). On the other hand, in the solid model the behaviour of the work-pieces can be modelled by a thermo-elasto-visco-plastic law. Then, the solid model is able to compute directly the residual stress. Figure 20 presents the value of the temperature and the von Mises stress over the control line of Fig. 21 with yield stress equal to 280 MPa and a rotation speed of 40 RPM at the end of the simulation (i.e. after 15 s). After a cooling period, the residual stresses are directly computed (see Fig. 22). The shape of the computed residual stresses corresponds to the classical shape observed after such a process [29,30].

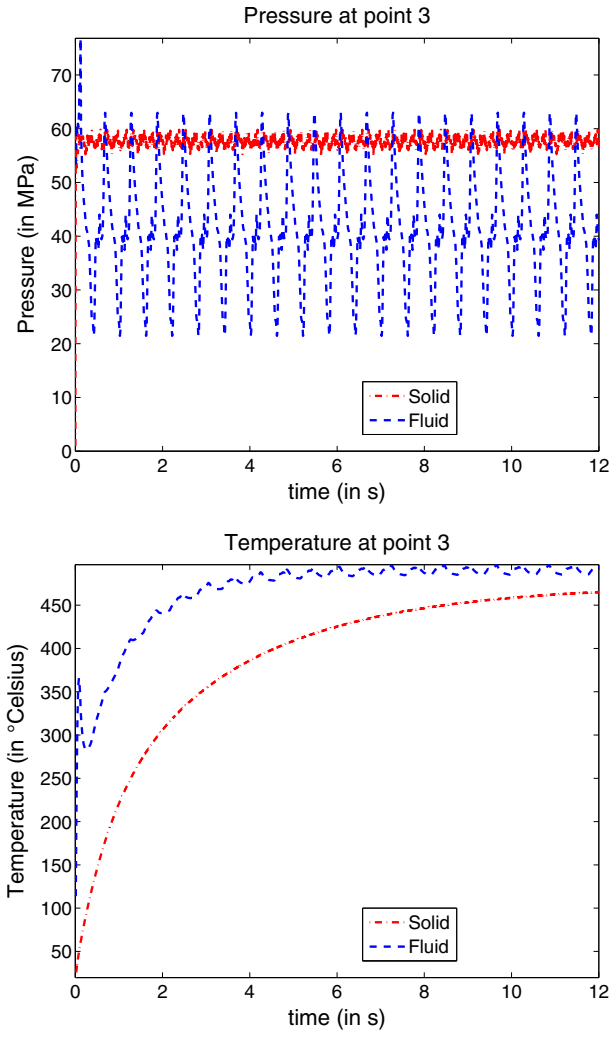

Fig. 14 Evolution of the pressure and the temperature computed by the two models at the control point 3 (fixed in space). The rotation speed of the tool is 100 RPM and the initial position of this point is defined in Fig. 5

The solutions with a rotation speed of 40 RPM are the extension in 3D of the results computed in 2D (see in [11]). The results computed by the 3D models are very different from the ones given by the 2D ones. The maximal temperature at points 1, 2 and 3 are respectively about 230 °C, 250 °C and 200 °C for the 3D models versus 140 °C, 110 °C and 105 °C in the case of the 2D models. These differences are explained by the approximations of the 2D models, like the effects of the shoulder and the thermal boundary conditions. Indeed, the shoulder that cannot be modelled in 2D has an important effect on the mechanical intermixing of the two materials, as well as on the value of the temperature field. The deformation rates in the neighbourhood of the shoulder are more important than the ones around the pin. Therefore, the main part of the heat generated during the FSW process is produced in the neighbourhood of the shoulder. Consequently, the heat generated by the shoulder explains that the values of the temperature fields computed

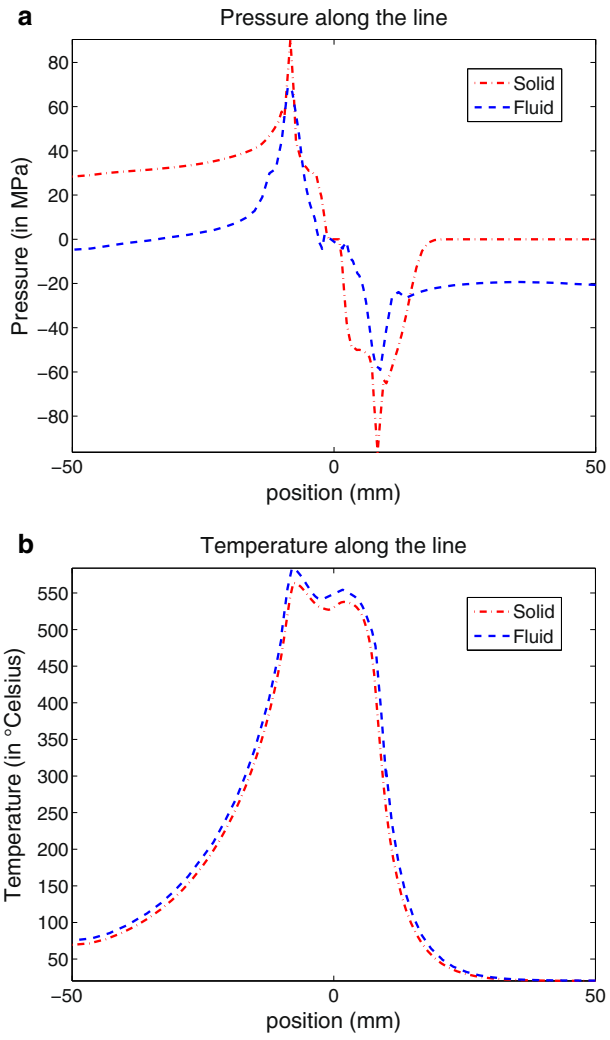

Fig. 15 Final values of the pressure and the temperature computed by the two models along the control line (i.e. after 12 s). The rotation speed of the tool is 100 RPM and the considered line is defined in Fig. 5

with 3D models are more important than the ones of 2D models. So it is clear that a 3D model is more relevant than a 2D model.

Conclusion

The phenomena happening during the friction stir welding (FSW) process are at the interface between solid mechanics and fluid mechanics. In this paper, two different formulations are presented to simulate the FSW process numerically. One 3D model is based on a solid approach which computes the position and the temperature fields and another one is based on a fluid approach written in terms of velocity, pressure and temperature fields. Both models use advanced numerical techniques such as the Arbitrary Lagrangian Eulerian formalism or remeshing operations or an advanced stabilization algorithm. These advanced numerical techniques allow the simulation of the FSW process with a tool with no rotational symmetry. The aim of the paper is to compare two computational models based respectively on a solid and a fluid approach for the solution of FSW process. Based

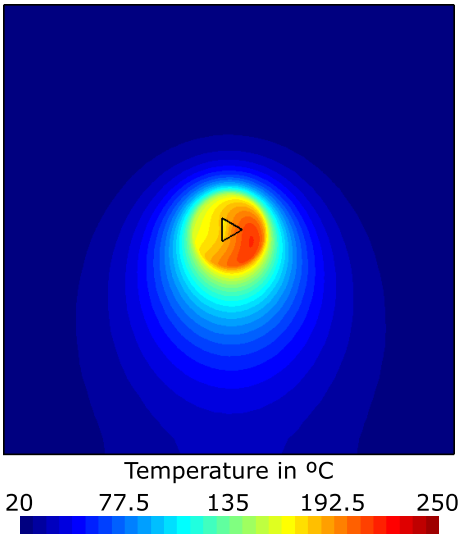

Fig. 16 Value of the temperature field computed by the solid model on the top of the plates at the end of the simulation (i.e. after 15 s). The rotation speed of the tool is 40 RPM

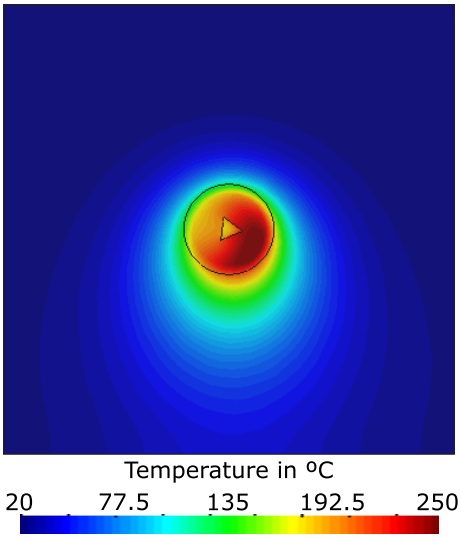

Fig. 17 Value of the temperature field computed by the fluid model on the top of the plates at the end of the simulation (i.e. after 15 s). The rotation speed of the tool is 40 RPM

on the authors' point of view, being able to simulate a process using a solid model and at the same time a fluid model, is numerically very interesting and represents a further verification of the implementation in both approaches. The presented example (with a triangular pin) shows that the two formulations essentially deliver the same results. Nevertheless, each model has its specificities. The computation of the next time step with the fluid model only requires the nodal values. The history of the internal variables is not necessary. This specificity allows the fluid model to use less CPU-intensive numerical techniques. Thus, the fluid model is more efficient from a computational point of view. The downside is that this model is limited to a thermo-visco-plastic constitutive model.

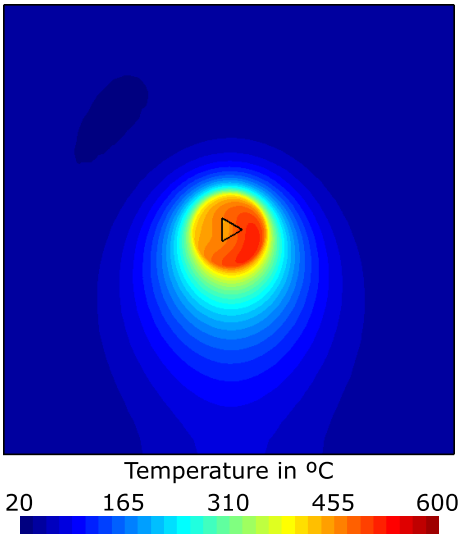

Fig. 18 Value of the temperature field computed by the solid model on the top of the plates at the end of the simulation (i.e. after 12 s). The rotation speed of the tool is 100 RPM

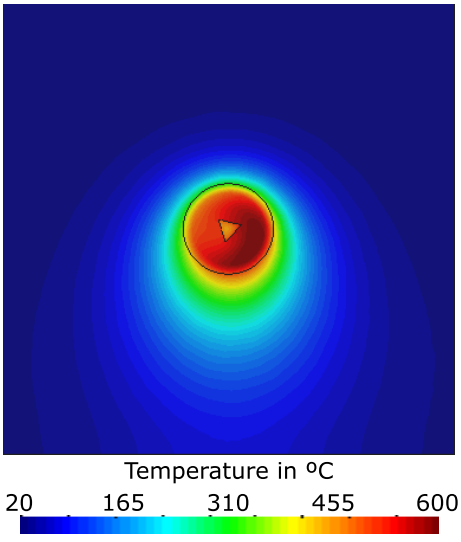

Fig. 19 Value of the temperature field computed by the fluid model on the top of the plates at the end of the simulation (i.e. after 12 s). The rotation speed of the tool is 100 RPM

Table 1 CPU time in hours versus the model type

Rotation speed	Solid model	Fluid model
40 RPM	59	37
100 RPM	131	79

On the other hand, the model based on the solid approach has the advantage that it can be used with any thermo-elasto-visco-plastic constitutive model. Therefore, the solid model can be used to predict the FSW process and to also compute the residual stresses after the end of the process.

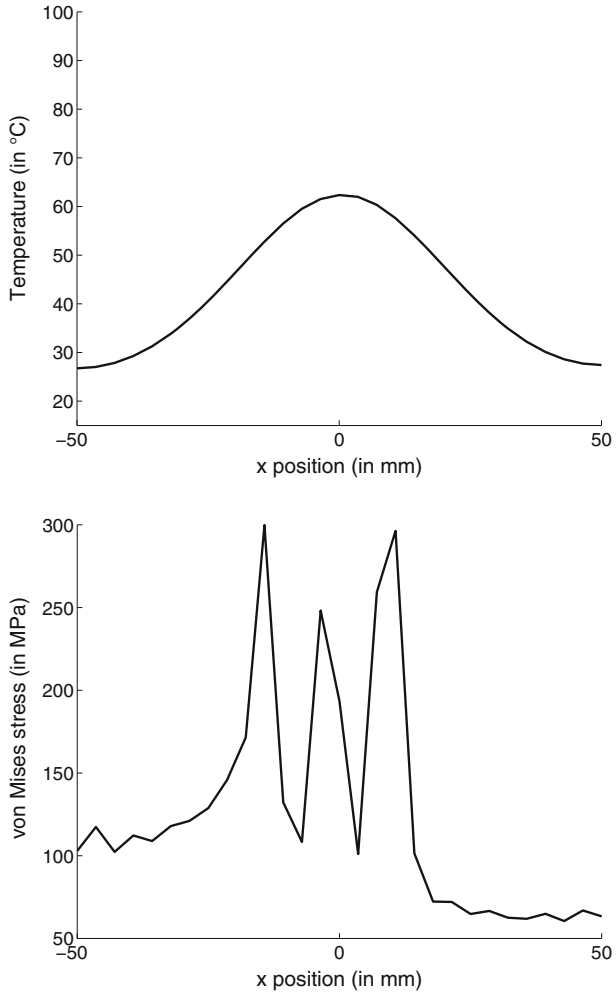

Fig. 20 Final values of the temperature and the von Mises stress computed by the solid models along the control line (i.e. after 15 s). The behaviour of the work-pieces is modelled by a thermo-elasto-visco-plastic law and the considered line is defined in Fig. 21

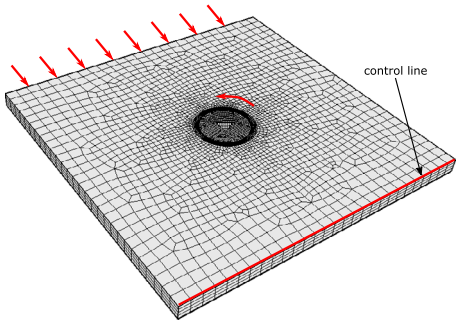

Fig. 21 Mesh of the solid model with the position of the control line used to plot the residual stress

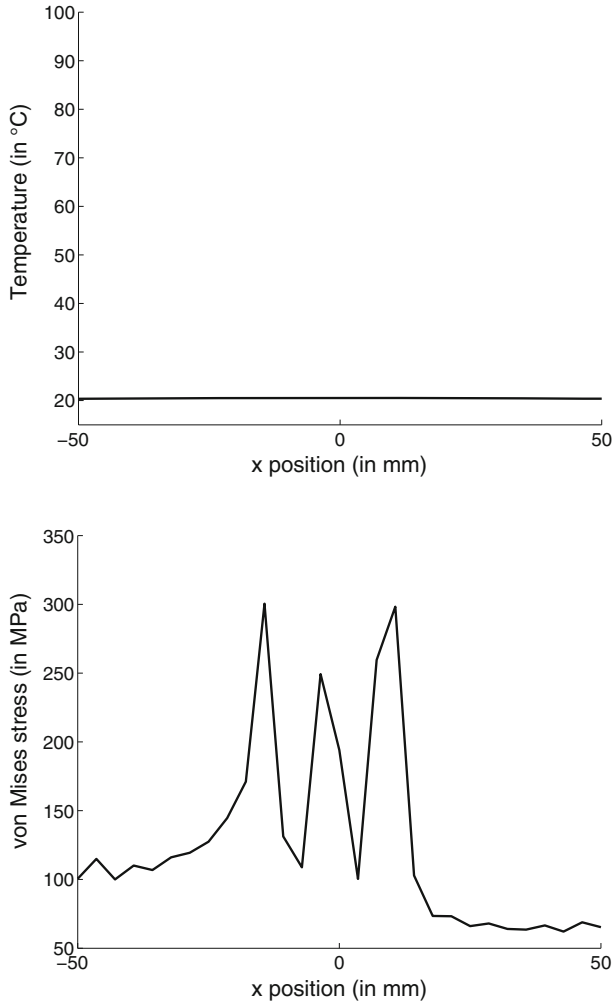

Fig. 22 Final values after cooling of the temperature and the von Mises stress computed by the solid models along the control line. The behaviour of the work-pieces is modelled by a thermo-elasto-visco-plastic law and the considered line is defined in Fig. 21

Authors' contributions
The Belgian authors worked on the model based on the solid approach and the Spanish authors worked on the one based on the fluid approach. All authors have read and approved the final manuscript

Author details
[1]Department of Aerospace and Mechanical Engineering, Non Linear Computational Mechanics, University of Liège, Quartier Polytech 1, Allée de la Découverte 13a, 4000 Liège, Belgium , [2]International Center for Numerical Methods in Engineering (CIMNE), Universidad Politécnica de Cataluña, Campus Norte UPC, 08034 Barcelona, Spain.

Acknowledgements
The Belgian authors wish to acknowledge the Walloon Region for its financial support to the STIRHETAL project (WINNOMAT program, convention number 0716690) and to the FSW-PME project (Programme de recherche collective 2013 – convention number 1217826) in the context of which this work was performed.

Competing interests
The authors declare that they have no competing interests.

Received: 30 May 2015 Accepted 15 October 2015
Published online: 18 November 2015

References

1. Thomas WM, Nicholas ED. Friction stir welding for the transportation industries. Mater Design. 1997;18(4–6):269–73. doi:10.1016/S0261-3069(97)00062-9.
2. Agelet de Saracibar C, Chiumenti M, Cervera M, Dialami N, Seret A. Computational modeling and sub-grid scale stabilization of incompressibility and convection in the numerical simulation of friction stir welding processes. Arch Comput Methods Eng. 2014;21(1):3–37. doi:10.1007/s11831-014-9094-z.
3. Feulvarch E, Roux J-C, Bergheau J-M. A simple and robust moving mesh technique for the finite element simulation of friction stir welding. J Comput Appl Math. 2013;246:269–77. doi:10.1016/j.cam.2012.07.013.
4. Dialami N, Chiumenti M, Cervera M, Agelet de Saracibar C, Ponthot, JP. Material flow visualization in friction stir welding via particle tracing. Int J Material Form. 2013. doi:10.1007/s12289-013-1157-4.
5. Assidi M, Fourment L, Guerdoux S, Nelson T. Friction model for friction stir welding process simulation: calibrations from welding experiments. Int J Mach Tools Manuf. 2010;50(2):143–55. doi:10.1016/j.ijmachtools.2009.11.008.
6. Santiago D, Lombera G, Urquiza S, Agelet de Saracibar C, Chiumenti M. Modelado termo-mecánico del proceso de friction stir welding utilizando la geometría real de la herramienta. Revista Internacional de Métodos Numéricos para Cálculo y Dise no en Ingeniería 26. 2010. p. 293–303
7. Buffa G, Fratini L, Arregi B, Penalva M. A new friction stir welding based technique for corner fillet joints: experimental and numerical study. Int J Material Form. 2010;3(1):1039–42. doi:10.1007/s12289-010-0948-0.
8. Heurtier P, Jones MJ, Desrayaud C, Driver JH, Montheillet F, Allehaux D. Mechanical and thermal modeling of friction stir welding. J Mater Process Technol. 2006;171(3):348–57. doi:10.1016/j.jmatprotec.2005.07.014.
9. He X, Gu F, Ball A. A review of numerical analysis of friction stir welding. Prog Mater Sci. 2014;65:1–66. doi:10.1016/j.pmatsci.2014.03.003.
10. Dialami N, Chiumenti M, Cervera M, Agelet de Saracibar C. An apropos kinematic framework for the numerical modelling of friction stir welding. Comput Struct. 2013;117:48–57. doi:10.1016/j.compstruc.2012.12.006.
11. Bussetta P, Dialami N, Boman R, Chiumenti M, Agelet de Saracibar C, Cervera M, Ponthot JP. Comparison of a fluid and a solid approach for the numerical simulation of friction stir welding with a non-cylindrical pin. Steel Res Int. 2014;85:968–79. doi:10.1002/srin.201300182.
12. Toumpis AI, Galloway AM, Arbaoui L, Poletz N. Thermomechanical deformation behaviour of dh36 steel during friction stir welding by experimental validation and modelling. Sci Technol Weld Join. 2014;19(8):653–63. doi:10.1179/1362171814Y.0000000239.
13. He W, Luan B, Xin R, Xu J, Liu Q. A multi-scale model for description of strain localization in friction stir welded magnesium alloy. Comput Mater Sci. 2015;104:162–71. doi:10.1016/j.commatsci.2015.04.002.
14. Simoes F, Rodrigues DM. Material flow and thermo-mechanical conditions during friction stir welding of polymers: literature review, experimental results and empirical analysis. Mater Design. 2014;59:344–51. doi:10.1016/j.matdes.2013.12.038.
15. Chiumenti M, Cervera M, Agelet de Saracibar C, Dialami N. Numerical modeling of friction stir welding processes. Comput Methods Appl Mech Eng. 2013;254:353–69. doi:10.1016/j.cma.2012.09.013.
16. Donea J, Huerta A, Ponthot JP, Rodríguez-Ferran A. Arbitrary Lagrangian Eulerian methods. In: Stein E, de Borst R, Hughes TJR, editors. Encyclopedia of Computational Mechanics. New York: Wiley;2004. doi:10.1002/0470091355.ecm009.
17. Boman R, Ponthot J-P. Efficient ALE mesh management for 3D quasi-eulerian problems. Int J Numer Methods Eng. 2012;92:857–90. doi:10.1002/nme.4361.
18. Boman R, Ponthot J-P. Enhanced ALE data transfer strategy for explicit and implicit thermomechanical simulations of high-speed processes. Int J Impact Eng. 2013;53:62–73. doi:10.1016/j.ijimpeng.2012.08.007.
19. Agelet de Saracibar C, Chiumenti M, Valverde Q, Cervera M. On the orthogonal subgrid scale pressure stabilization of finite deformation J2 plasticity. Comput Methods Appl Mech Eng. 2006;195:1224–51. doi:10.1016/j.cma.2005.04.007.
20. Cervera M, Chiumenti M, Valverde Q, Agelet de Saracibar C. Mixed linear/linear simplicial elements for incompressible elasticity and plasticity. Comput Methods Appl Mech Eng. 2003;192:5249–63.
21. Chiumenti M, Valverde Q, Agelet de Saracibar C, Cervera M. A stabilized formulation for incompressible plasticity using linear triangles and tetrahedra. Int J Plast. 2004;20:1487–504. doi:10.1016/j.ijplas.2003.11.009.
22. Agelet de Saracibar C, Cervera M, Chiumenti M. On the formulation of coupled thermoplastic problems with phase-change. Int J Plast. 1999;15:1–34.
23. Cervera M, Agelet de Saracibar C, Chiumenti M. Thermo-mechanical analysis of industrial solidification processes. Int J Numer Methods Eng. 1999;46:1575–91.
24. Bussetta P, Boman R, Ponthot J-P. Efficient 3D data transfer operators based on numerical integration. Int J Numer Methods Eng. 2015;102(3–4):892–929. doi:10.1002/nme.4821.
25. Ponthot JP. Unified stress update algorithms for the numerical simulation of large deformation elasto-plastic and elasto-viscoplastic processes. Int J Plast. 2002;18:91–126. doi:10.1016/S0749-6419(00)00097-8.
26. Simar A, Pardoen T, de Meester B. Effect of rotational material flow on temperature distribution in friction stir welds. Sci Technol Weld Join. 2007;12(4):324–33. doi:10.1179/174329307X197584.
27. Gerlich A, Yamamoto M, North TH. Strain rates and grain growth in Al 5754 and Al 6061 friction stir spot welds. Metall Mater Trans A. 2007;38(6):1291–302. doi:10.1007/s11661-007-9155-0.
28. Guerra M, Schmidt C, McClure JC, Murr LE, Nunes AC. Flow patterns during friction stir welding. Mater Charact. 2002;49(2):95–101. doi:10.1016/S1044-5803(02)00362-5.
29. Hattel JH, Sonne MR, Tutum CC. Modelling residual stresses in friction stir welding of al alloys-a review of possibilities and future trends. Int J Adv Manuf Technol. 2015;76(9–12):1793–805. doi:10.1007/s00170-014-6394-2.
30. Sonne MR, Tutum CC, Hattel JH, Simar A, de Meester B. The effect of hardening laws and thermal softening on modeling residual stresses in FSW of aluminum alloy 2024–T3. J Mater Process Technol. 2013;213(3):477–86. doi:10.1016/j.jmatprotec.2012.11.001.